Green Chemistry

Accepted Manuscript

This article can be cited before page numbers have been issued, to do this please use: S. Meher and R. K. Rana, *Green Chem.*, 2019, DOI: 10.1039/C9GC00116F.

ROYAL SOCIETY OF CHEMISTRY

rsc.li/green-chem

ROYAL SOCIETY OF CHEMISTRY View Article Online
DOI: 10.1039/C9GC00116F

Journal Name

ARTICLE

A Rational Design of Pd-based Catalyst with Metal-Metal Oxide Interface Influencing the Molecular Oxygen in Aerobic Oxidation of Alcohols†

Received 00th January 20xx,
Accepted 00th January 20xx

DOI: 10.1039/x0xx00000x

www.rsc.org/

Songhita Meher,[a,b] Rohit Kumar Rana*,[a,b]

In a green process for selective oxidation of alcohols, the utilization of molecular oxygen as primary oxidant is the most critical step. Although many palladium (Pd)-based catalysts have shown potential, the role of different Pd-species in the aerobic oxidation reaction is still a matter of discussion. There have been diverse reports, which describe either Pd^0 or Pd^{2+} as individual species responsible for the aerobic oxidation of alcohols. Herein we demonstrate that the presence of both Pd^0 and Pd^{2+} species with Pd-PdO interface stabilized on the surface of reduced graphene oxide (rGO) is important for the oxidation of alcohols. With an optimum Pd^{2+}/Pd^0 ratio, the catalyst catalyzes oxidation of benzyl alcohol in water with oxygen, resulting in a turnover frequency (TOF) of up to 18000 h^{-1} with 98% selectivity towards the aldehyde. It is proposed that both metallic Pd and its oxide domains, when co-exist with a phase boundary between them, they promote the activation of oxygen. On the other hand, the rGO provides surface functionalities for the formation and stabilization of Pd-PdO nanoclusters enabling the catalyst to be both stable and reusable. Using histidine as a scavenger for singlet oxygen, we have also determined the importance of oxygen-activation in the reaction. Furthermore, the catalyst is capable of converting various other alcohols into the corresponding carbonyl compounds. Comparison of various catalysts shows that the Pd-PdO@rGO catalyst is the most efficient in terms of TOF, conversion and selectivity for the oxidation of benzyl alcohol using oxygen than the reported Pd-based catalysts, particularly when performed under milder reaction conditions. Therefore, the result on Pd-catalyst designing is believed to be of significance for the further developments in the environmentally benign oxidation processes involving molecular oxygen as the oxidant.

Introduction

Selective oxidation of alcohols to their corresponding carbonyl compounds is one of the important organic reactions in the synthesis of fine chemicals and intermediates.[1] Normally, the classical oxidation methods used for such reactions involve stoichiometric amount of inorganic oxidants, such as, permanganate or chromate reagents producing large amounts of toxic waste.[2,3] Considering the ever increasing environmental concerns, it is now paramount that alternative oxidation processes are developed, which would be environmental friendly apart from being efficient. In particular, the utilization of molecular oxygen as the primary oxidant in these reactions besides the usage of water as the solvent is considered extremely critical. Amongst the various catalysts explored, the palladium (Pd)-based nanomaterials have shown immense potential in enabling oxygen as the oxidant in the reaction. It includes a wide variety of reactions, such as, epoxidation of alkenes, oxidation of CO, hydrocarbon, alcohol, glucose, *etc*.[4-12]

In the Pd-catalysts, the main focus has been to tailor their particle size, surface structure, morphology and the supporting matrix, so as to improve their activities in the oxidation reactions. The various materials used for the support include hydroxyapatite, Al_2O_3, MgO, mesoporous silica, carbon, and graphene for dispersing and stabilizing the Pd nanoparticles on their surface.[9,13-16] Conventionally high surface area and porous materials are used as the support. Although the role of these supports is mainly to prevent agglomeration of the metallic nanoparticles, there are other effects which can influence the catalytic activity. For example, the use of some of the metal oxides as support has demonstrated the importance of charge transfer between metal and oxide in the oxidation reaction under O_2.[4] Metal organic framework (MOF) structures have also been utilized as support for metal nanomaterials, wherein it is believed to allow generation of a large number of

[a] Nanomaterials Laboratory, CSIR-Indian Institute of Chemical Technology, Hyderabad-500007, India.
[b] Academy of Scientific and Innovative Research (AcSIR), Ghaziabad- 201002, India.
CSIR-IICT Communication Number: IICT/pubs/2018/336
E-mail: rkrana@iict.res.in

†Electronic Supplementary Information (ESI) available: Experimental details of the sample preparation; Details of the equipments used for characterization and analyses; FE-SEM, HR-TEM, EDS, XRD, XPS data of various samples; Characterization of Pd nanoparticles; Comparison with the catalytic activities reported for other catalysts. See DOI: 10.1039/x0xx00000x

active sites in the framework with a controllable space for chemical reactions to take place.[17] In another approach to provide anchoring sites for the formation and immobilization of metal nanoparticles, organic materials like mesoporous ionic copolymer are used as the supporting matrix.[18] Similarly, it has been reported that doped nitrogen atoms in carbon as support can facilitate enhancement of the electron density of Pd^0 resulting in increased reaction rate.[14]

From a rational catalyst-design point of view, the Pd based materials should enable the oxygen activation, which is the key for the catalytic performance.[4] The oxygen is activated from its ground state (triplet) to a high energy state (singlet) *via* Pd–O_2 interaction, which in turn enables it to participate in the oxidation reaction. As this interaction requires electron transfer from Pd surface to O_2, the variation in Pd surface charge density can play an influential role. Therefore, use of a support matrix that can suitably polarise the Pd particles at their interfaces would be beneficial. In this context, the graphene-based materials with their high electronic conductivity along with the effective surface area and good mechanical strength, can be apt for the designing of Pd-based catalysts.[19]

Recent reports on graphene based compositions as the support for Pd have revealed their potential in the aerobic oxidation of alcohols. Luque *et. al.* used a surfactant-mediated method to prepare Pd particles of ~40 nm sizes deposited on graphene oxide (GO).[20] Thus obtained catalyst exhibited a yield of 98% corresponding to a TOF of 175 h^{-1} in the aerobic oxidation of benzyl alcohol to benzaldehyde. Li's group demonstrated deposition of Pd nanoparticles of ~4.1 nm sizes on reduced graphene oxide (rGO) via an impregnation method followed by two separate heat treatments at 300 °C under He flow and 10% H_2/He flow.[21] The catalyst showed a conversion of 73% in the aerobic oxidation of benzyl alcohol at 110 °C. Although, there was a partial oxidation of the Pd^0 to Pd^{2+} as observed in the used catalyst, the catalytic activity was attributed to Pd^0 only, wherein the presence of graphene was thought to promote the reaction *via* efficient adsorption of the alcohol and oxygen. In a similar approach, Wang's group could prepare sub-nanometer sized Pd particles on rGO *via* impregnation and then heat-treatments in presence of H_2.[22] But, contrasting to previous result, herein the observed catalytic activity with a TOF of 1960 h^{-1} was attributed to the presence of Pd^{2+} species coordinated with Cl^- ions rather than the Pd^0 species.

Although, there have been investigations to find out the nature of the Pd species, their role in the aerobic oxidation reaction is still a matter of discussion. It should be noted that the Pd-based catalysts, which are mainly reported for the liquid-phase aerobic oxidation of alcohols, have been prepared with the major emphasis on the formation of Pd in its metallic state (Pd^0) except a few on Pd^{2+}.[4,11,13,22,23] However, while designing the catalysts, the importance of the composition and the oxidation state of palladium desirable for activation of molecular oxygen has rarely been given the due consideration. This prompted us to focus on a rational designing of the Pd based nanomaterials in order to achieve efficient catalytic activity and selectivity in the aerobic oxidation reactions, while bringing out the role of various Pd species in the reaction. In a somewhat similar context, as known in case of the automotive exhaust catalysis, which is done under gas-phase requiring high reaction temperature and oxygen pressure, the composition of the Pd-based catalysts play an important role in the reaction.[24] It has been proposed that both metallic Pd and its oxide domains, when co-exist in a polycrystalline particle with a phase boundary between them, they can promote the activation of molecular oxygen. From the thermodynamics point of view, it has also been predicted that the adhesion energy for the Pd and PdO can favourably form a stable interface.[25] During the catalytic reactions, the Pd-PdO interface is believed to allow the surface reduction of PdO *via* its interaction with Pd^0 to form oxygen vacancy (Pd-O*) sites.[26] This Pd-O* sites then facilitate the adsorption and activation of molecular oxygen.

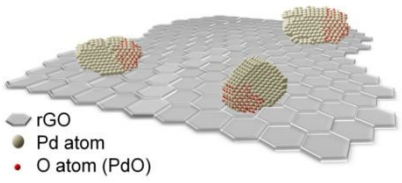

Scheme 1. Schematic representation illustrating the Pd-based catalyst designed to have exposed Pd-PdO interfaces stabilized on the surface of rGO.

Therefore, in the present study, to design and understand the role of the active Pd species in the reaction under oxygen, we prepared catalysts based on various Pd-PdO compositions. The formation and stability of Pd-PdO interface is also a challenge as the inter-convertibility of the metal-metal oxide during the reaction can concomitantly lead to loss in catalytic activity. Herein, we utilize the surface functionalities present on partially reduced exfoliated graphene oxide (rGO) sheets to effectively stabilize Pd-PdO nanoparticles (Scheme 1). The catalyst preparation is done under mild reaction conditions without using any stabilizing agent or surfactant, in which the GO is first partially reduced in order to provide optimum oxygen functionalities as anchoring sites for a better dispersion of the palladium precursor. Then, an *in-situ* reduction process leads to the formation of Pd-PdO composition on the rGO surface. The rGO is used not only to stabilize and promote the Pd-PdO nanoparticles in the catalytic reaction, but also to provide a hydrophobic–hydrophilic balance desirable for efficient interaction of the organic substrate with the catalyst surface.[27]

Experimental

Materials

Graphite flakes (25 μm), $KMnO_4$, $N_2H_4.H_2O$, Na_2PdCl_4, K_2CO_3, Benzyl alcohol and dialysis sacks (12000 Da MWCO) were purchased from Sigma-Aldrich and used as received. DI (Deionized) water (18.2 MΩ) was used for all the solution preparation.

Synthesis of Pd-PdO@rGO

An aqueous dispersion of graphene oxide (80 mL, 1 mg/mL) (see ESI†) was prepared *via* sonication using bath sonicator for 30 min. For partial reduction of GO, 0.1 mL of hydrazine hydrate (80 v/v % in water) was added drop-wise to the above suspension and stirred for 1 h. In a typical synthesis for Pd loading on rGO, 0.940 mL of Na_2PdCl_4 (10 mM) was added slowly to the above suspension followed by the addition of hydrazine hydrate (0.1 mL, 80 v/v % in water). Then it was exposed to high-intensity ultrasonic irradiation (20 KHz, 40% intensity, Sonic Vibro cell, USA) under ambient air for 30 min at 25 °C. The resulted black precipitate was centrifuged followed by washing with DI water for five times to obtain Pd-PdO@rGO. Thus obtained material was re-dispersed in DI water to prepare a stock solution of 10 mg/mL. As confirmed from ICP-OES analysis, there was no Pd-precursor remained in the filtrate. The Pd-loading was varied from (0.625 to 5.0 Wt.%) by taking different amounts of Na_2PdCl_4 and keeping all other parameters same as above. The catalysts are denoted as Pd-PdO@rGO-x, where x represents Pd-loadings in Wt.%. As found from the ICP-OES analysis, the total Pd-loading in Pd-PdO@rGO varied from 0.625 to 5.0 Wt.% (Table S1).

Catalytic oxidation of aromatic alcohols under O_2

Oxidation of aromatic alcohols over various catalysts was performed under O_2 atmosphere and water as the solvent. In each experiment, 20 mg of the catalyst was used in 5 mL of DI water and mixed with 0.3 mol of K_2CO_3 under stirring at 800 rpm/min. Then at a desirable reaction temperature, 0.1 mol of the reactant was added into the reaction mixture and the reaction was carried out using oxygen balloon. The products formed at various time intervals were analyzed by gas chromatography (GC) equipped with ZB-5 column.

Reusability of the catalyst

To check the reusability of the catalyst, the catalyst after a fixed duration of the reaction was separated and washed with ethyl acetate and then with water for 2-3 times. Thus separated catalyst was then used in the next cycle for benzyl alcohol oxidation keeping the reaction conditions similar.

Results and Discussion

Designing the Catalyst

During the preparation of the catalyst, we observed that the reduction of GO to rGO was a critical step, which influenced the dispersion of Pd-PdO particles on its surface. When the reduction of both GO and Pd^{2+} ions was carried out simultaneously, it resulted in non-uniform and agglomerated Pd-PdO particles on the reduced GO (Fig. S1a). Since the oxygenated functionalities present on GO provide anchoring sites for the Pd^{2+} species to interact with the support, the amount or the localized concentration of such functionalities must be affecting the Pd-PdO dispersion on the surface of the graphene sheets. Therefore, in a control experiment we first allowed the GO to be partially reduced prior to their interaction with the Pd^{2+} precursor. The reduction process was monitored by analyzing the oxygenated functional groups present in GO using FT-IR spectroscopy (Fig. 1(a)). In case of GO, the bands at 1750 cm^{-1} and 1630 cm^{-1} corresponding to C=O stretching of carboxylic and carbonyl functional groups, respectively were observed. The presence of other oxygen containing functionalities in GO, such as the alkoxy and epoxide groups were revealed from the C-O stretching vibrations at 1100 cm^{-1} and 1240 cm^{-1}, respectively. After the GO was partially reduced, there was a decrease in the intensities of the vibrational bands corresponding to the above oxygen containing functional groups confirming the conversion of GO to its reduced form rGO.

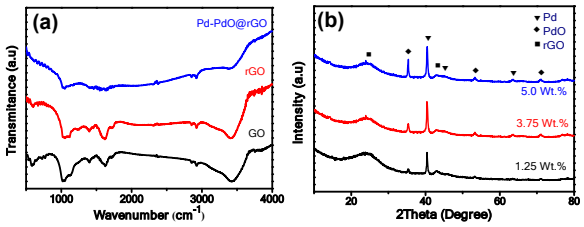

Fig. 1 (a) FT-IR spectra of GO, rGO and Pd-PdO@rGO-1.25; (b) XRD patterns of Pd-PdO@rGO samples with different Pd-loadings (Wt.%).

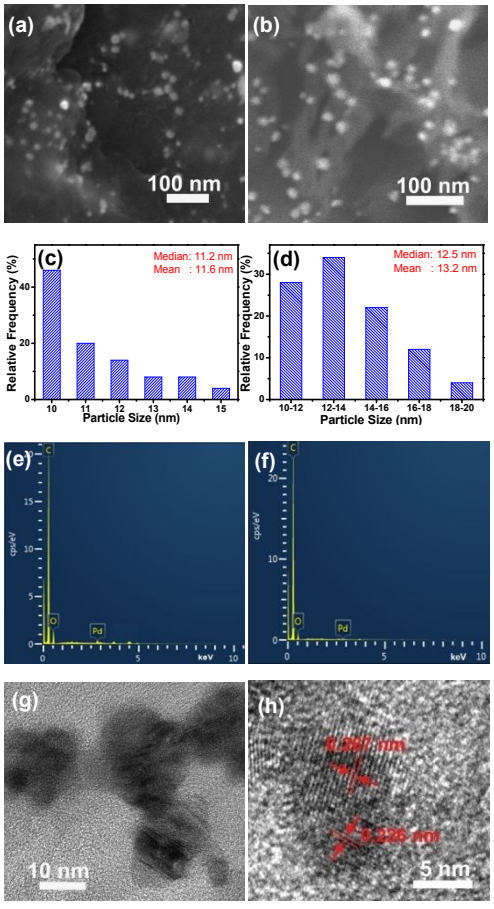

Fig. 2 FE-SEM images of Pd-PdO@rGO with Pd-loadings of (a) 0.625 Wt.% and (b) 1.25 Wt.% and the corresponding (c, d) particle-size distribution plot (from a count of >50 particles), respectively; (e, f) EDS of Pd-PdO@rGO-1.25 and Pd-PdO@rGO-0.625; (g), HRTEM image and (h) the corresponding HRTEM image of the highlighted (red circle) part depicting the lattice fringes of Pd and PdO crystallites in Pd-PdO@rGO-1.25.

Thus prepared rGO was then used along with the Pd^{2+} precursor and subjected to the reduction process again for the synthesis of Pd-PdO@rGO. This resulted in further decrease in the intensity or disappearance of the FT-IR bands due to the oxygen containing functionalities (Fig. 1(a)).

The as-synthesized materials were further characterized by X-ray diffraction technique. The XRD pattern of the prepared GO sample showed a typical weak, but broad diffraction centred at 26.4° corresponding to the graphitic (002) plane, while the known interlayer graphitic (100) diffraction peak at 11.7° was absent (Fig. S1(b)). This indicated that the insertion of oxygen functionalities had successfully led to exfoliation of the graphitic sheets.[28,29] The XRD pattern also remained similar for the rGO prepared via the reduction of GO (Fig. S1(b)). In case of Pd-PdO@rGO-x samples ("x" indicates Pd-loadings in terms of total Pd-content in Wt.%), the broad diffraction seen at 26.4° clearly indicated the presence of exfoliated graphene sheets (Fig. 1(b)). The diffraction peaks observed at 40.4, 45.5 and 79o were assigned to the (111), (200) and (311) planes, respectively, of metallic Pd with a face-centered cubic lattice. In addition, we observed the diffraction peaks at 35.5, 54.3, 64.6 and 71.8o, which could be indexed to the (101), (112), (103) and (202) planes, respectively, of PdO with a tetragonal lattice.[30] Thus the XRD data revealed the formation of both Pd and PdO in the as-synthesized Pd-PdO@rGO. The crystallite sizes of these particles were then estimated using the Debye-Scherrer equation. For Pd and PdO, the crystallite sizes were in the range of 2.4-2.78 and 0.54-0.65 nm, respectively (Table S2). It was also observed that the intensity of the corresponding XRD peaks due to Pd and PdO increased with increase in the Pd-loading.

The morphological characterization of Pd-PdO@rGO was carried out using FE-SEM and HR-TEM. The FE-SEM images and the corresponding particle-size distribution plots for Pd-PdO@rGO samples with different Pd-loadings showed that particles of sizes 10-15 nm having distinctly high contrast were present on sheet-like structures of rGO (Fig. 2(a-d)). As determined from the EDS analysis, we found the presence of Pd, C (carbon) and O (oxygen) in these samples (Fig. 2(e, f), Table S2), while the particles mainly consisted of Pd (Fig. S2). Further analysis by EDS for elemental mapping showed a homogeneous distribution of the Pd along with the other elements. The average size for the Pd-containing particles as estimated from the size-distribution plot was ~11 nm for the Pd-PdO@rGO sample with a Pd-loading of 0.625 Wt.% (Fig. 2c). As we increased the Pd-loading the sizes of these nanoparticles increased reaching to a value of ~40 nm for the sample with 5.0 Wt.% loading (Fig. S2 (d,e)).

The HRTEM analysis of Pd-PdO@rGO sample also showed the presence of Pd-containing particles with dark contrast and their sizes were in the range of 10-15 nm (Fig. 2(g)). At a higher magnification, the HRTEM image displayed the lattice fringes for these particles (Fig. 2(h), Fig. S3). The lattice fringe with an interplanar distance (d-spacing) of 0.226 nm could be indexed to the (111) plane of Pd metal, while the d-spacing of 0.267 nm corresponded to the (101) plane of PdO with a tetragonal lattice. The presence of both Pd and PdO in the sample also corroborates well with the observation made from XRD data. We further analysed the sample by high-angle annular dark-field scanning transmission electron microscopy (HAADF STEM) and elemental mapping (Figure S4). The elemental mapping for O and Pd in the STEM image shows that there are regions having both Pd and O elements indicative of PdO content in the sample. The other regions, wherein Pd is predominant represent the presence of Pd component in the sample. Therefore, the result further supports the formation Pd-PdO interface in the synthesized materials. It further reveals that the nano-sized metallic Pd and PdO co-exist with an interface between them. Importantly, these Pd-PdO interfaces are seen to remain exposed at their surface and hence should be accessible to the reactants as desirable for the catalytic oxidation reaction under oxygen atmosphere. We could rule out the possibility of any core–shell morphology or an oxide layer formation on the Pd metal surface as known in case of the catalyst prepared at elevated temperatures, which would otherwise obstruct the Pd-PdO interface to be exposed to the reactants.[23]

In order to obtain information on the structure and quality of the graphene-based materials and their reduction during the synthesis of Pd-PdO@rGO, we analyzed the as-synthesized materials by confocal micro-Raman spectroscopy. The Raman spectra of Pd-PdO@rGO, rGO and GO samples are shown in Fig. 3. Graphene-based materials generally exhibit two characteristic modes (G and D) of vibration.[19] While the D-band corresponds to out-of-plane vibrations attributed to the presence of structural defects, the G-band is a result of in-plane vibrations of carbon atoms in the graphene structure. In case of GO and rGO-containing samples (rGO and Pd-PdO@rGO), the D and G bands appear within a range of 1298-1330 cm^{-1} and 1533-1590 cm^{-1}, respectively. The intensity ratio of the D and G bands (I_D/I_G) as a measure of the reduction process, was seen to increase in the following order, GO (1.28) < rGO (1.46) < Pd-PdO@rGO (1.59). This gradual increase in the ratio with reduction suggests that more graphitic domains are being formed as a result of the effective reduction of the oxygenated functionalities present on GO.[31] Moreover, the shift in the G band position towards lower wavenumber in case of Pd-PdO@rGO also reflects a more ordered graphitic structure in this material than that in rGO and GO samples.[32]

The chemical composition and surface functional groups present in Pd-PdO@rGO was investigated by X-ray photoelectron spectroscopy. Especially in case of GO or rGO, the binding energy of C1s electron is useful in identifying the various types of carbon attached with oxygen and therefore can provide information on the GO-reduction process. The deconvoluted C1s spectrum for GO revealed five different peaks with binding energies of 284.4, 285.3, 286.2, 286.7, and 288.2 eV (Fig. 4(a)). These binding energies correspond to graphitic carbon C=C, C-C, and carbon bound to oxygen species (C-O (hydroxyl and epoxy), C=O (carbonyl), and O-C=O (carboxyl) groups), respectively.[33]

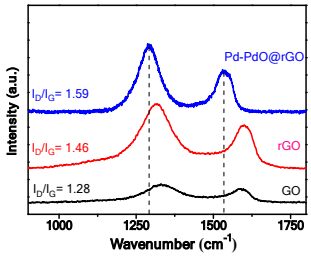

Fig. 3 Confocal micro-Raman spectra of GO, rGO and Pd-PdO@rGO-1.25.

Table 1 The C:O and Pd^{2+}:Pd^0 ratio obtained from the XPS analysis of various samples

Sample	Oxidized carbon to graphitic carbon ratio (C1S)	C1S/O1S ratio	Pd^{2+}/Pd^0 ratio
GO	1.14	2.07	-
Pd-PdO@rGO-0.625	0.88	2.89	0.21
Pd-PdO@rGO-1.25	0.92	3.02	0.33
Pd-PdO@rGO-5	0.90	2.98	0.96

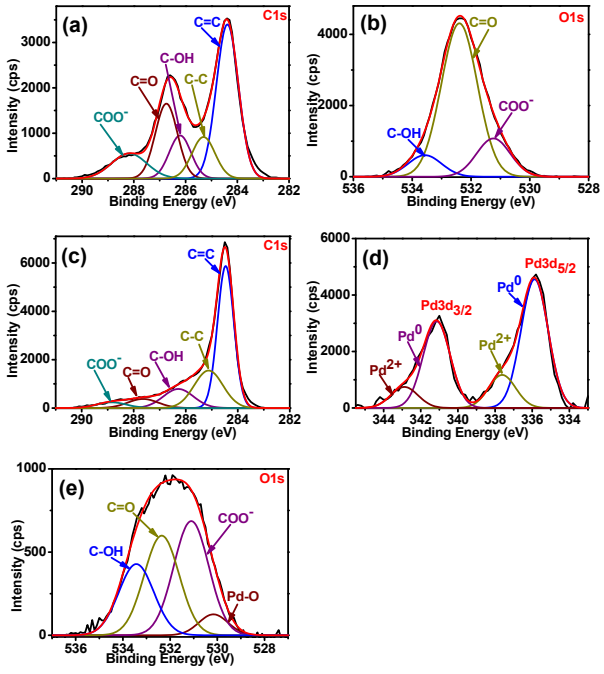

Fig. 4 XPS analysis showing (a) C1s and (b) O1s spectra for GO sample; (c) C1s, (d) O1s and (e) Pd 3d spectra for Pd-PdO@rGO-1.25 sample.

The O1s spectrum for GO also showed the presence of three oxygen-containing functionalities with binding energies of 531.1 eV (COO^-), 532.36 eV (C=O) and 533.43 eV (C-OH) (Fig. 4(b)). In case of the Pd-PdO@rGO samples, we observed a decrease in the intensity of the C1s peaks particularly for the carbon bound to oxygen functionalities (Fig. 4(c)). When it was compared with that of GO, clearly there was a decrease in the intensity ratio of the oxygen-containing carbon with respect to the graphitic carbon in Pd-PdO@rGO (Table 1). In addition, as estimated from the total C1s and O1s (oxygen attached with carbon) peak areas, the ratio of carbon to oxygen (C/O) was found to increase from a value of 2.07 in GO to 3.02 in Pd/PdO@rGO Therefore, the decrease in the oxygen containing functionalities in Pd-PdO@rGO further substantiates the data obtained from Raman analysis on the formation of rGO.

The spectrum corresponding to Pd 3d electron for Pd-PdO@rGO consisted of two sets of peaks indicating that the palladium exists in two different oxidation states (Fig. 4(d)). The one with binding energies at 335.87 and 341.14 eV was assigned to $Pd3d_{5/2}$ and $Pd3d_{3/2}$ electrons in Pd metal (Pd^0). The other set having $Pd3d_{5/2}$ and $Pd3d_{3/2}$ peaks at 337.62 and 342.88 eV revealed the presence of Pd^{2+} state as PdO.[34] A quantitative analysis of the XPS peaks shows that in case of Pd-PdO@rGO, the metallic Pd content is more than that of the oxide form (Pd^{2+}) as present on the surface of the catalyst. Moreover, with increase in the Pd-loading in the catalyst, the Pd^{2+} : Pd^0 ratio was found to increase from a value of 0.21 to 0.96 (Table 1, Fig. S5). Similarly, the estimation of Pd and PdO content by the XRD analysis also showed an increase in the PdO content as the Pd-loading was increased (Table S3, Supporting Information). Moreover, the percentage of Pd content obtained from XRD analysis was found to be higher than that was estimated from the XPS analysis. This result indicates that the percentage of PdO is more on the surface compared with that in the bulk of the sample. The presence of both Pd and PdO also supports the observation made from HRTEM analyses. The XPS for O1s also showed the presence of a peak at 530.16 eV corresponding to PdO besides three other components assignable to the oxygen-containing functionalities (Fig. 4(e), Fig. S5).

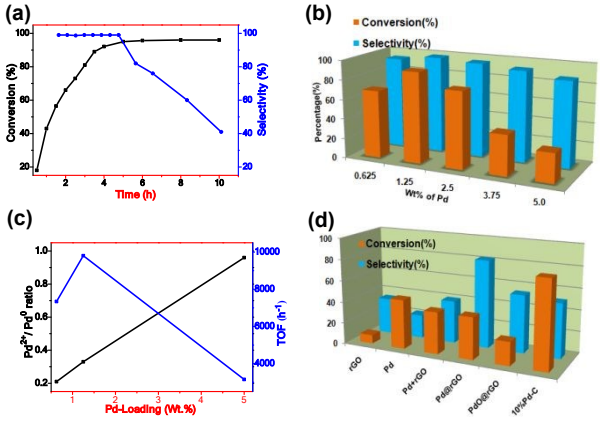

Fig. 5 (a) Time-dependent reaction progress for the catalytic conversion of benzyl alcohol and the selectivity towards benzaldehyde; (b) Conversion and selectivity with respect to different Pd-loading in Pd-PdO@rGO as catalyst; (c) Plot representing the catalytic activity (TOF in sec^{-1}) and the variation in PdO/Pd ratio with respect to different Pd-loading in Pd-PdO@rGO as catalyst; (d) Conversion and selectivity with respect to different catalysts. Reaction conditions: Catalyst (2.35μmol of Pd-content), 0.1 mol benzyl alcohol, 0.3 mol K_2CO_3, 5 mL water, O2 (~1atm), 80 °C, 4h.

Catalytic activity of Pd-PdO@rGO in the oxidation of alcohols

Catalytic activity of the prepared catalysts was tested in oxidation of both aromatic and aliphatic alcohols using molecular oxygen as the oxidant and water as the solvent. In order to optimise the reaction conditions, we varied the experimental parameters, such as, temperature, catalyst amount and reaction duration using benzyl alcohol as the

View Article Online
DOI: 10.1039/C9GC00116F

model substrate (Table S4). When the reaction temperature was increased from 25 °C to 100 °C, though there was a gradual increase in the conversion, the highest selectivity (98.2%) towards benzaldehyde was observed at a temperature of 80°C (Table S4). The reaction is known to proceed via a two-step mechanism. The 1st step, the base in the reaction promotes deprotonation of the Pd-bound alcohol and then the β-H elimination reaction in presence of oxygen results in benzaldehyde.[23] In the 2nd step, the aldehyde undergoes hydration to form geminal diol followed by its dehydrogenation to the corresponding carboxylic acid. Therefore, the decrease in selectivity observed at temperatures above 80 °C could be due to the facilitation of the 2nd step of the reaction. Higher rates of aldehyde oxidation have also been observed in cases where the hydration equilibrium is shifted towards the geminal diol catalyzed by strong bases and at higher temperatures.

We also studied other solvent systems in the reaction keeping the temperature fixed at 80 °C. Amongst the various solvents used, water was found to be the most suitable in achieving both higher conversion and selectivity (Table S4). Besides the solubility of oxygen, water is also reported to provide appropriate wetness of the surface facilitating chemisorption of O_2 as required for good activity.[37,38] The variation in the catalyst (Pd-PdO@rGO-1.25) amount showed that with increase in its amount from 10 mg to 40 mg, there was an increase in the conversion from 83.0% to 98.5%, but, the selectivity towards benzaldehyde decreased from 98% to 61% as the higher amount of catalyst allowed over-oxidation of the product.

Table 2 Effect of composition, surface area and particle-size on the catalytic activity of various catalysts in the oxidation of benzyl alcohol[a]

Catalyst	Pd-loading (Wt.%)	Pd-PdO Particle-size (nm)	Surface area (m^2/g)	Conv.[b] (%)	Select.[c] (%)	TOF (h^{-1})
Pd-PdO@rGO-0.625	0.625	10-15	260	69	93.6	7343
Pd-PdO@rGO-1.25	1.25	10-20	211	92.1	98.26	9801 18304[d]
Pd-PdO@rGO-2.5	2.5	20-25	199	78	96	8301
Pd-PdO@rGO-3.75	3.75	_	101	41	92.6	4363
Pd-PdO@rGO-5	5.0	40-50	98	29.6	87	3150

[a] Reaction conditions: Catalyst (2.35 µmol of Pd-content), 0.1 mol benzyl alcohol, 0.3 mol K_2CO_3, 5.0 mL water, O_2 (~1atm), 80 °C, 4h. [b] Conversion determined by GC, [c] Selectivity towards Benzaldehyde, [d]TOF estimated for 1h of the reaction.

The optimum catalyst amount was 20 mg, which resulted in 92.1% conversion and 98.2% selectivity for benzaldehyde within 4h of reaction. The time profile of the reaction involving the Pd-PdO@rGO catalyst in the conversion of benzyl alcohol and the selectivity to benzaldehyde in water under oxygen atmosphere is shown in Fig. 5(a). The conversion increased with time and reached the maximum at 4 h. After 4h there was no obvious change seen in the conversion, but, further oxidation of the benzaldehyde led to decrease in its selectivity. The other products were identified as benzoic acid and benzyl benzoate.

It was observed that either in absence of any catalyst or rGO as the catalyst, there was no or only a negligible amount of product formed under similar reaction conditions (Table S5). This clearly indicates that the presence of Pd-PdO nanoparticles deposited on rGO is responsible for achieving the higher conversions in the oxidation of benzyl alcohol. The catalytic conversion, selectivity and turnover frequency (TOF) for all the Pd-PdO@rGO-x catalysts are compared in Table 2 (Fig. 5(b), Fig. S6). With increase in the Pd-loading from 0.625 to 1.25 Wt.%, there was an increase in the activity, but further increase in loading led to decrease in the activity. Apart from the differences in Pd-PdO particle-size and surface area, the increased PdO:Pd ratio could be one of the reasons for the lower activity seen at higher Pd-loadings (Table 2, Fig. 5(c)). In case of the catalyst with lowest Pd-content (0.625 Wt.%), despite having the textural properties similar to that for Pd-PdO@rGO-1.25, the catalytic activity was low. This further strengthens the importance of PdO:Pd ratio in the activity of the catalyst. The Pd-PdO@rGO with 1.25 Wt.% Pd-loading was found to be the optimum composition with PdO:Pd of 0.33 for obtaining the highest activity within 4 h of reaction time and the major product obtained was benzaldehyde with a selectivity of 98.2%.

The effect of both Pd and PdO in the catalytic reaction was further investigated. In two separate controlled conditions, we prepared catalysts with either Pd or PdO nanoparticles (experimental section). The Pd nanoparticles with sizes of ~15 nm, prepared via a reduction process (Fig. S7), showed 46% conversion with 22% selectivity towards benzaldehyde (Fig. 5(d), Table S5). When the Pd nanoparticles were physically mixed with rGO, it still displayed an almost similar conversion as that of unsupported Pd nanoparticles, but, with a slightly better (40%) selectivity. The better selectivity observed in the presence of rGO could be due to its hydrophobicity preventing the possibility of hydration of the benzaldehyde and its further oxidation.[27] The selectivity towards benzaldehyde could be improved further by an *in-situ* deposition of Pd nanoparticles on rGO (Pd@rGO) (Fig. 5(d), Fig. S8, Table S5). However there was no further improvement in the conversion for the

View Article Online
DOI: 10.1039/C9GC00116F

Pd@rGO catalyst. Under the same reaction conditions, the commercially available Pd/C (Pd-loading of 10 Wt.% on carbon) exhibited 81% conversion with 51% selectivity towards benzaldehyde (Fig. 5(d), Table S5). On the other hand, when the metal oxide was deposited on rGO (PdO@rGO, Fig. S8), both the conversion and selectivity for the catalyst still remained in the lower side (Fig. 5(d), Table S5). Therefore, the higher activities observed in Pd-PdO@rGO could be due to the presence of Pd-PdO composition in the catalyst. Especially, the generation of Pd-PdO interface is the crucial step in influencing the catalytic activity. It provides the active sites suitable for achieving better conversion and selectivity in the oxidation reactions involving molecular oxygen as the oxidant.

Table 3 Oxidation of various alcohols using Pd-PdO@rGO-1.25 as the catalyst[a]

Entry	Substrate	Conv. (%)	Select. (% aldehyde)	TOF (h^{-1})
1	4-methoxy benzyl alcohol	80	100	8524
2	3-methyl benzyl alcohol	69	73.9	7343
3	4-fluoro benzyl alcohol	41	73.4	4363
4	1-phenyl ethanol	79	95.1	8407
5	Furfuryl alcohol	82	97.5	8726
6	2-thiophene methanol	59	85.6	6279
7	Cyclooctanol	73	94.5	7769
8	Cyclohexanol	78	100	8301
9	± Menthol	68	87.8	7237
10	1-heptanol	83.5	85	8886
11	6-mercapto1-hexanol	53.5	76.6	5693
12	Crotyl alcohol	81	96.3	8620

[a]Reaction conditions: 20 mg catalyst (Pd-PdO@rGO-1.25), 0.1 mol alcohol, 0.3 mol K_2CO_3, 5 mL water, O_2 (~1atm), 80 °C, 4h.

As known in metal-metal oxide systems, the interface between Pd and PdO can play an important role in O_2 activation.[39] Particularly, the work functions of the metal and oxide that allows the charge transfer at their interface is ascribed as one of the major factors responsible for their catalytic activity and selectivity. As discussed earlier, the electronic interaction at Pd-PdO interface can result in oxygen vacancies, which then allows adsorption and activation of the molecular oxygen as required in the catalytic oxidation reactions.[28] Moreover, it is also known that the surface charge density of metals can be influenced by the graphene support, which in turn can contribute to the oxygen activation.[21,40] As observed from the variation in Pd-loading, an optimum ratio of PdO:Pd is necessary for the best catalytic activity, while at higher percentage of Pd-loading the increased PdO amount in the catalyst becomes detrimental to the catalytic activity. In order to determine the role of the generated reactive oxygen species, we performed the catalytic reaction in presence of a scavenger for singlet oxygen ($^1O_2$). It has been well established that histidine with its imidazole side chain is susceptible towards singlet oxygen and hence used as a scavenger or quencher.[41,42] We observed that the presence of histidine resulted in a drastic decrease in the catalytic activity of the Pd-PdO@rGO catalyst in the aerobic oxidation of benzyl alcohol (Table S6). This finding indicates that the adsorbed oxygen species on the catalyst surface, plausibly in a similarity to the singlet oxygen, are quenched by the histidine.[41]

The performance of the Pd-PdO@rGO-1.25 catalyst was then investigated in the oxidation of other aromatic and aliphatic alcohols (Table 3). In case of the para-substituted benzyl alcohols, the catalytic activity was found to follow the Hammett rule. Accordingly, substitution with electron donating groups like -OCH_3 and -CH_3 showed better catalytic activity compared with that for electron withdrawing groups (-F). However, owing to the stereic effect of these substituents, the overall activity was found to be lower than that for un-substituted benzyl alcohol. The catalyst was also effective in the oxidation of heterocyclic alcohols, such as furfuryl alcohol and thiophene-2-methanol (Table 3, entries 5 and 6). For the non-aromatic alcohols, both cyclic and linear forms could be selectively oxidized to the corresponding aldehydes using the Pd-PdO@rGO-1.25 as catalyst (Table 3, entries 7-11). Moreover, in case of an unsaturated linear compound (crotyl alcohol, entry 12), the observed selective oxidation of the alcohol group further expands the scope of this catalyst. It was noted that similar selectivity via oxidative dehydrogenation by Pd-based catalysts were reported earlier, but the presence of surface oxide rather than the metallic Pd was attributed for the catalytic activity.[14,44] The presence of sulphur in the compound (entry 6 and 11) resulted in lower activity indicating that the unshared electron pairs present on sulphur keeps these compounds strongly bound to the metal surface thereby preventing their oxidation.[45]

Catalytic stability and reusability of Pd-PdO@rGO

In order to gain insight into the stability and reusability, we first investigated the heterogeneous nature of the Pd-PdO@rGO catalyst. This was done by separating the catalyst from the reaction mixture in the middle of the catalytic reaction (at 2 hr) at the reaction temperature of 80 oC. The reaction was then continued in absence of the solid catalyst. As shown in Fig. 6(a), the reaction initially progressed with increase in the conversion till 2h, but, after that as the catalyst was removed there was no further increase in the conversion. Analysis of the reaction mixture by ICP-OES did not show any presence of leached palladium. Therefore, the observed conversion of benzyl alcohol in the oxidation reaction is clearly associated with the Pd-PdO@rGO catalyst, in which the Pd-PdO particles are well stabilized on the rGO, and as a result it exhibits a typical heterogeneous catalytic behaviour.

A significant advantage of heterogeneous catalysts is the ease of their separation from the reaction mixture and their reuse in subsequent reactions. Therefore, to test the reusability of the catalyst, it was separated from the reaction mixture and washed for further use in the next reaction cycles. As tested for 5 cycles, the Pd@rGO-1.25 catalyst could retain its activity without any significant loss in both conversion and selectivity (Fig. 6(b)). There was also no leaching of the Pd species as determined from the ICP-OES analysis of the reaction medium during different cycles. We further characterized the used catalyst by FE-SEM, XRD, XPS, micro-Raman spectroscopy and electron microscopy (Fig. 7, Fig. S9). The presence of both Pd

metal and PdO in the used catalyst could be seen from the XRD and XPS analyses (Fig. 7(a,b)). Accordingly, in the HRTEM image, the lattice fringes corresponding to the (111) plane of Pd metal and (101) plane of PdO could also be seen in the used catalyst (Fig. 7(c,d)). Importantly, the presence of Pd-PdO interface in the used catalyst as desirable for the catalytic activity could also be confirmed in the HRTEM images. The average Pd-PdO particle-size was in the range of ~12.8 nm (Fig. S9(c)). The graphitic structure of rGO in the used catalyst was analyzed by the Raman analysis, which showed a I_D/I_G ratio of 1.54 (Fig. S9(d)). The XPS results further showed a PdO:Pd ratio of 0.32 and a C:O ratio of 2.93 indicating that the composition and morphology of the catalyst remained almost similar to that of the fresh catalyst (Table S7, Fig. S10).

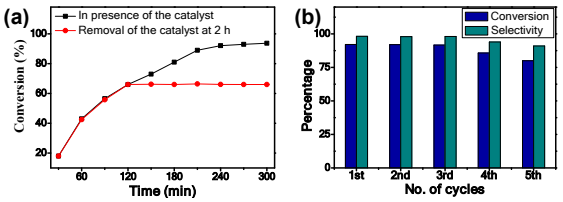

Fig. 6 (a) Comparison of the reaction progress with time wherein the catalyst is removed after 2h of the reaction to determine the heterogeneous catalytic behaviour of the catalyst; (b) Recyclability of the catalyst showing catalytic activity at various reaction cycles. Reaction conditions: 20 mg catalyst (Pd-PdO@rGO-1.25), 0.1mol benzyl alcohol, 0.3 mol K_2CO_3, 5 mL water, O_2 (~1atm), 80 °C.

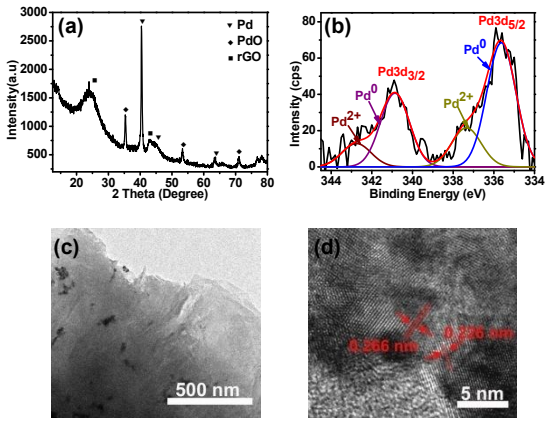

Fig. 7 Characterization of the used Pd-PdO@rGO-1.25 catalyst; (a) XRD pattern; (b) XPS for Pd 3d electrons; (c) HR-TEM image; (d) HR-TEM image depicting the lattice fringes for Pd and PdO crystallites.

It should be noted that in comparison to the various reported Pd-based heterogeneous catalysts, the present catalyst exhibits activity and selectivity (TOF= 18001 h^{-1} at 1 h) comparable to the best ones for the benzyl alcohol oxidation in presence of oxygen (Table S8). Moreover, to the best of our knowledge, particularly amongst the reported aerobic oxidation reactions carried out under mild reaction conditions, the performance of the present catalyst is the most efficient in terms of conversion, selectivity and TOF. While this activity could be attributed to the controlled formation of Pd-PdO on the surface of rGO, in case of most of the reported catalysts, the focus had been to prepare metallic (Pd0) nanoparticles.[4] Interestingly, though in some of the cases both Pd^0 and Pd^{2+} species were present in the catalysts, the catalytic activity was attributed only to the individual species.[1-3] In the present case, the results demonstrate the importance of both Pd metal and its oxide with Pd-PdO in designing the catalysts for improved activity and selectivity, but also with required stability to be used as a recyclable heterogeneous catalyst in the oxidation reactions involving molecular oxygen as the oxidant.

Conclusions

In this work, we demonstrated a rational designing for Pd-based catalysts in selective oxidation of alcohols using oxygen desirable for catalytic oxidation processes. It involved an *in-situ* method to control the interfacial assembly of Pd-PdO on the rGO surface without using any external reagents like surfactants or templates. The method resulted in the formation of Pd-PdO composite nanoparticles with a distinct interface between them and well dispersed on the surface of the graphene sheets. Thus obtained Pd-PdO@rGO exhibited efficient catalytic activity and selectivity in the oxidation of benzyl alcohol to benzaldehyde under O_2 atmosphere and in water as the solvent. The presence of Pd-PdO was found to be the key in influencing the catalytic reaction involving the molecular oxygen as the oxidant. Moreover, the hybrid catalyst could also be used in catalyzing oxidation of varieties of other alcohols. Therefore, while these findings bring out the importance of Pd-PdO interface and its stabilization on the rGO to achieve enhanced catalytic activity in oxidation reactions under O_2 as the oxidant, the catalyst designing is anticipated to further aid in developing environmentally benign chemical processes for the oxidation reactions. The conclusions section should come in this section at the end of the article, before the acknowledgements.

Conflicts of interest

There are no conflicts to declare.

Acknowledgements

The work was supported by CSIR, India (FTT, MLP-0024) and DST, India (Nanomission, SR/NM/NS-111/2010). S.M. acknowledges CSIR, India (SRF) for the fellowship. The authors are grateful to Dr. S.V. Manorama, Dr. Gousia Begum, Y. Swarnalatha, B. Arun Kumar and Bikash Sharma for helping in materials characterization.The acknowledgements come at the end of an article after the conclusions and before the notes and references.

Notes and references

1. M. Hudlicky, ACS Monograph Series, American Chemical Society: Washington, DC, **1990**.
2. G.Cainelli,; G.Cardillo, , Springer: Berlin, **1984**.
3. D. G. Lee and U. A. Spitzer, *J. Org. Chem.* 1970, **35**, 3589.

4. R. Long, H. Huang, Y. Li, L. Song and Y. Xiong, *Adv. Mater.* 2015, **27**, 7025–7042.
5. S. Hayashi, H. Yorimitsu and K. Oshima, *J. Am. Chem. Soc.* 2009, **131(6)**, 2052–2053.
6. F. Rumpf, H. Poppa and M. Boudart, *Langmuir.* 1988, **4(3)**, 722–728.
7. J. Long, H. Liu, S. Wu, S. Liao and Y. Li, *ACS Catal.* 2013, **3**, 647−654.
8. D. I. Enache, J. K. Edwards, P. Landon, B. Solsona-Espriu, A. F. Carley, A. A. Herzing, M. Watanabe, C. J. Kiely, D. W. Knight and G. J. Hutchings, *Science.* 2006, **311(5759)**, 362–365.
9. K. Mori, T. Hara, T. Mizugaki, K. Ebitania and K. Kaneda, *J. Am. Chem. Soc.* 2004, **126**, 10657–10666.
10. M. Besson, F. Lahmer, P. Gallezot, P. Fuertes and G. Fleche, *J. Catal.* 1995, **152**, 116–121.
11. P. Xin, J. Li, Y. Xiong, X. Wu, J. Dong, W. Chen, Y. Wang, L. Gu, J. Luo, H. Rong, C. Chen, Q. Peng, D. Wang and Y. Li, *Angew. Chem. Int. Ed.* 2018, **57**, 4642–4646.
12. B. Hao, M. Xiao, Y. Wang, H. Shang, L. Ma,Jun and H. Yang Mao, *ACS Appl. Mater. Interfaces*, 2018, **10**, 34332−34339.
13. S. F. J. Hackett, R. M. Brydson, M. H. Gass, I. Harvey, A. D. Newman, K. Wilson and A. F. Lee, *Angew. Chem. Int. Ed.* 2007, **46**, 8593–8596.
14. P. Zhang, Y. Gong, H. Li, Z. Chen and Y. Wang, *Nat. Commun.,* 2013, **4**, 1593-1–11.
15. U**.** R. Pillai and E. Sahle-Demessie, *Green Chem.* 2004, **6**, 161–165.
16. C. M. A. Parlett, D. W. Bruce, N. S. Hondow, A. F. Lee and K. Wilson, *ACS Catal.,* 2011, **1**, 636–640.
17 S. Proch, J. Herrmannsdörfer, R. Kempe, C. Kern, A. Jess, L. Seyfarth, J. Senker, *Chem. Eur. J.,* 2008, **14**, 8204–8212
18 Q. Wang, X. Cai, Y. Liu, J. Xie, Y. Zhou, J. Wang, *Appl. Catal. B*, 2016, **189**, 242–251
19. B. Qiu, M. Xing and J. Zhang, *Chem. Soc. Rev.,* 2018, **47**, 2165–2216.
20. S. Rostamnia, E. Doustkhah, Z. Karimi, S. Amini and R. Luque, *ChemCatChem*, 2015, **7**, 1678 –1683.
21. G. Wu, X. Wang, N. Guan and L. Li, *Appl. Catal. B.,* 2013, **136–137***,* 177–185.
22. L. Lei, Z. Wu, R. Wang, Z. Qin, C. Chen, Y. Liu, G. Wang, W. Fan and J. Wang, *Catal. Sci. Technol.,* 2017, **7**, 5650–5661.
23. J. D. Grunwaldt, C. Matteo and B. Alfons, *J. Phys. Chem. B.*,2006, **110(51)**, 25586–25589.
24. H. Xiong, K. Lester, T. Ressler, R. Schlögl, L. F. Allard and A. K. Datye, *Catal. Lett.,* 2017, **5**, 1095–1103.
25. C. T. Campbell, *Phys Rev Lett*., 2006, **96**, 066106-1–4.
26. M. M. Wolf, H. Zhu, W. H. Green and G. S. Jackson, *Appl. Catal. A.,* 2003, **244**, 323–340.
27. B. Karimi, M. Khorasani, H. Vali, C. Vargas and R. Luque, *ACS Catal.,* 2015, **5**, 4189−4200.
28. S. Stankovich, D. A. Dikin, R. D. Piner, K. A. Kohlhaas, A. Kleinhammes, Y. Jia, Y. Wu, S. T. Nguyen and R. S. Ruoff, *Carbon,* 2007, **45(7)**, 1558−1565.
29. J. Zhao, Z. Liu, H. Li, W.Hu, C. Zhao, P. Zhao and D. Shi, *Langmuir,* 2015, **31**, 2576−2583.
30. A. Baylet, P. Marecot, D. Duprez, P. Castellazzi, G. Groppi and P. Forzatti, *Phys. Chem. Chem. Phys.,* 2011, **13**, 4607−4613.
31. A. C. Ferrari and J. Robertson, *Phys. Rev. B.,* 2000, **61**, 14095–14107.
32. J. Ma, A. Habrioux, Y. Luo, L. Ramos-Sanchez, L. Calvillo, G. Granozzi, P. B. Balbuena and N. Alonso-Vante, *J. Mater. Chem. A.,* 2015, **3**, 11891-11904.
33. D. R. Dreyer, S. Park, W. B. Christopher and R. S. Ruoff, *Chem. Soc. Rev.,* 2010, **39**, 228–240.
34. Q. Lv, Q. Meng, W. Liu, N. Sun, K. Jiang, L. Ma, Z. Peng, W. Cai, C. Liu, J. Ge, L. Liu and W. Xing, *J. Phys. Chem. C.,* 2018, **122**, 2081−2088.
35. J. A. Mueller, C. P. Goller and M. S. Sigman, *J. Am. Chem. Soc.* 2004, **126**, 9724−9734.
36. D. Anna, M. M. Mali, M. Mastrorilli, P. Cotugno and P. A. Monopoli, *J. Mol. Catal. A.,* 2014, **386**, 114−119.
37. M. Musawir, P. N. Davey and G. K. I. V. Kozhevnikov, *Chem. Commun.,* 2003, **0**, 1414–1415.
38. T. L. Stuchinskaya and I. V. Kozhevnikov, *Catal. Commun*., 2003, **4**, 417–422.
39. (a) G. A. Somorjai and J. Y. Park, *Angew. Chem*. *Int. Ed*. 2008, **47**, 9212; (b) Y. G. Wang, Y. Yoon, V. A. Glezakou, J. Li and R. *J.* Rousseau, *Am. Chem. Soc*., 2013, **135**, 10673.
40. B. Liu, P. Wang, A. Lopes, L. Jin, W. Zhong, Y. Pei, S. L. Suib, J. He, *ACS Catal.,* 2017, **7**, 3483
41. P. L. Hartmanz, A. Artma and K. Aul, *Photochem. Photobiol.,* 1990, **51**, 59-66.
42. I. B. C. Matheson, R. D. Etheridge, N. R. Kratowch and J. Lee, *Photochem. Photobiol.,* 1975, **21**, 165-171.
43. R. Long, K. Mao, X. Ye, W. Yan, Y. Huang, J. Wang, Y. Fu, X. Wang, X. Wu, Y. Xie and Y. Xiong, *J. Am. Chem. Soc.,* 2013, **135**, 3200.
44. A. F. Lee, C. V. Ellis, J. N. Naughton, M. A. Newton, C. M. A. Parlett and K. *J.* Wilson, *Am. Chem. Soc.,* 2011, **133**, 5724–5727.
45. L. J. Hoyos, M. Primet and H. Praliaud, *J. Chem. Soc. Faraday Trans.,* 1992, **88(1)**, 113-119.

View Article Online
DOI: 10.1039/C9GC00116F

Journal Name

ARTICLE

Graphical Abstract